Pharmacokinetic Evaluation of the Penetration of Antituberculosis Agents in Rabbit Pulmonary Lesions

Maria C. Kjellsson,[a,b] Laura E. Via,[c] Anne Goh,[d] Danielle Weiner,[c] Kang Min Low,[d] Steven Kern,[a] Goonaseelan Pillai,[a] Clifton E. Barry III,[c] and Véronique Dartois[d]

Modeling & Simulation, Novartis Pharma AG, Basel, Switzerland[a]; Department of Pharmaceutical Biosciences, Uppsala University, Uppsala, Sweden[b]; Tuberculosis Research Section, Laboratory of Clinical Infectious Disease, National Institute of Allergy and Infectious Diseases, National Institutes of Health, Bethesda, Maryland, USA[c]; and Novartis Institute for Tropical Diseases, Pharmacology Unit, Singapore[d]

Standard antituberculosis (anti-TB) therapy requires the use of multiple drugs for a minimum of 6 months, with variable outcomes that are influenced by a number of microbiological, pathological, and clinical factors. This is despite the availability of antibiotics that have good activity against *Mycobacterium tuberculosis in vitro* and favorable pharmacokinetic profiles in plasma. However, little is known about the distribution of widely used antituberculous agents in the pulmonary lesions where the pathogen resides. The rabbit model of TB infection was used to explore the hypothesis that standard drugs have various abilities to penetrate lung tissue and lesions and that adequate drug levels are not consistently reached at the site of infection. Using noncompartmental and population pharmacokinetic approaches, we modeled the rate and extent of distribution of isoniazid, rifampin, pyrazinamide, and moxifloxacin in rabbit lung and lesions. Moxifloxacin reproducibly showed favorable partitioning into lung and granulomas, while the exposure of isoniazid, rifampin, and pyrazinamide in lesions was markedly lower than in plasma. The extent of penetration in lung and lesions followed different trends for each drug. All four agents distributed rapidly from plasma to tissue with equilibration half-lives of less than 1 min to an hour. The models adequately described the plasma concentrations and reasonably captured actual lesion concentrations. Though further refinement is needed to accurately predict the behavior of these drugs in human subjects, our results enable the integration of lesion-specific pharmacokinetic-pharmacodynamic (PK-PD) indices in clinical trial simulations and in *in vitro* PK-PD studies with *M. tuberculosis*.

It takes 6 to 9 months of combination four-drug pharmacotherapy to cure drug-sensitive tuberculosis (TB), despite the availability of antibiotics that have bactericidal activity *in vitro*. Even such long and intensive treatment with multiple complementary drugs has not prevented the emergence and spread of resistant forms of bacilli (61). In contrast, other pulmonary infectious diseases can be cured in a few days to a few weeks with single drugs that have MICs against the corresponding pathogen comparable to those of first-line anti-TB agents. The low efficiency of TB therapy is thought to be due to multiple factors, including high bacterial loads, the slow growth of the organisms interspersed with periods of dormancy, and the presence of persisters, whereby some bacterial subpopulations found in lesions have adapted to local microenvironmental conditions to become phenotypically drug resistant (23, 39, 48). This aspect of mycobacterial physiology has been intensively researched. One alternative explanation for the protracted chemotherapy, which has been overlooked to a large extent, concerns the penetration—or lack thereof—of anti-TB agents in the tissue compartments where pulmonary lesions and associated bacteria reside. A key distinction between TB and other pulmonary diseases is the nature and extent of the pathology that develops in response to infection with *Mycobacterium tuberculosis* in the human lung (12, 32). Pulmonary lesions are very diverse, both structurally and biochemically. The most common types observed in humans and higher species, such as the rabbit or nonhuman primates, are activated cellular granulomas, more differentiated granulomas with central necrosis and caseation, and fully mature cavities which are fibrotic. In addition, each of these lesion types is in turn quite heterogeneous. A good illustration of intralesional heterogeneity is the mature necrotic granuloma, made of a central caseous core surrounded by concentric cuffs of macrophages and lymphocytes encased in a fibrotic rim. The diversity of TB lesions and lesion compartments begs the question of drug access to these various sites of infection.

There have been few studies published from the 1950s to the 1980s indicating that drug concentrations in these remote target sites can be substantially lower than plasma concentrations and could also be different for different drugs (3, 6, 29, 30). These studies were limited to isoniazid (INH) and rifampin (RIF) and relied on microbiological readouts or unspecific radiochemical methods for the quantification of these drugs in plasma and tissues. Hence, there is a need to refine and expand studies of drug penetration in pulmonary TB lesions using sensitive analytical technologies and pharmacokinetic (PK) models of drug distribution. More recently, Ellard and colleagues examined drug penetration into the cerebrospinal fluid (CSF) in tuberculosis meningitis patients (14, 15). They observed that INH and pyrazinamide (PZA) achieved CSF concentrations similar to those observed in serum, while RIF penetrated slowly into the meninges, with maximal CSF levels of 0.4 to 0.8 μg/ml, only slightly above its MIC (0.3

TABLE 1 Plasma and pulmonary tissue pharmacokinetic studies conducted in MTB exposed NZW rabbits[a]

Drug(s) administered (no. of animals)	Dosing regimen	Sampling times	No., type, and diam of granulomas sampled
INH, RIF, PZA, and MXF ($n = 13$)	All 4 drugs given once to each animal at the following doses: INH, 50 mg/kg; RIF, 30 mg/kg; PZA, 125 mg/kg; MXF, 25 mg/kg	Plasma samples at 2-4 practical times during the expt; tissue samples at euthanasia (between 0.5 and 7 h)	46 solid granulomas, 1 to 4 mm
INH ($n = 4$)	30 mg/kg daily for 8 days	Plasma samples at 0, 0.5-1, and 1-2 h; tissue samples at euthanasia (between 2 and 4 h)	8 caseous, 1.5 to 3 mm; 3 suppurative, 1.5 to 3 mm
RIF ($n = 4$)	24 mg/kg daily for 8 days	Plasma samples at 0, 0.5-1, and 1-2 h; tissue samples at euthanasia (between 1 and 3 h)	3 solid, 1 to 4 mm; 3 caseous, 2.5 to 3 mm; 3 suppurative, 1.5 to 3 mm
INH, RIF, PZA, and MXF ($n = 12$)	All 4 drugs given to each animal once daily for 5 to 6 days: INH, 50 mg/kg; RIF, 30 mg/kg; PZA, 125 mg/kg; MXF, 25 mg/kg	Plasma samples at 2 to 4 practical times during the expt; tissue samples at euthanasia (between 1 and 17 h)	24 solid, 1 to 4 mm; 25 caseous, 1.5 to 4 mm; 5 suppurative, 1 to 2.5 mm; 6 coalescing, >4 mm, irregular shape; 2 cavity caseous cores, ND; 3 cavity walls, ND

[a] For each study, serial plasma samples were drawn before euthanasia. Pulmonary tissue samples were obtained at study end. ND, not determined.

μg/ml), occurring between 2 and 5 h after dosing. Observed CSF concentration-to-serum concentration ratios for RIF ranged from 0.04 to 0.11.

Differential lesion-specific penetration is likely to be important in TB disease since lesion size, location, structure, and cellular/noncellular content are remarkably diverse. Granulomas that appear early in the progression of the disease are small and mainly cellular before evolving into closed, caseous, necrotic lesions that often develop a wall of fibrosis (32). These lesions may evolve further due to liquefaction of the necrotic center, ultimately leading to the formation of cavities open to an airway. On the other hand, effective containment by the immune system can lead to partial healing, fibrosis, calcification, and the formation of consolidated, closed lesions. Due to various levels of vascularization and presence of physical barriers, the extent of sequestration of the bacilli and, therefore, the ability of drugs to access them are expected to differ among lesion types and even lesion compartments (5).

The rabbit model of *M. tuberculosis* infection recapitulates many of the human pathological features of TB disease (13). Progressive pulmonary infection with *M. tuberculosis* HN878 is characterized by the development of heterogeneous lesions within the same animal, similar to those described in the human lung: solid granulomas or nodules that are exclusively cellular and may coalesce upon disease progression, granulomas containing a caseous necrotic center, and older fibrotic lesions showing neovascularization. In addition, a subset of granulomas undergoes suppuration (liquefaction), eventually giving rise to cavities surrounded by a thick fibrotic wall (27). Determining drug levels in cavities is of significant interest because (i) they can harbor permissive macrophages and neutrophils supporting the growth of *M. tuberculosis* in very large numbers at the luminal surface (16, 26) and (ii) the presence and extent of cavitary disease have often been cited to be predictors of a poor clinical outcome, the development of resistance, and relapse (9, 28). Overall, the diversity of lesion types seen in the rabbit model makes it a useful tool for evaluating the ability of existing agents and new drug candidates to reach the site of action in human pulmonary TB.

In this study, we explored the ability of anti-TB agents to penetrate into both healthy lung tissue and different histopathologi-

cally defined types of TB lesions. We selected four antituberculosis drugs, three of which are first-line agents used for treating drug-sensitive TB in humans: INH, RIF, and PZA. The fourth agent is among the most efficacious second-line drugs used against multidrug-resistant TB: moxifloxacin (MXF). We report the plasma, lung, and lesion pharmacokinetics of these four drugs following single- and multiple-dose administration to *M. tuberculosis*-infected rabbits. The rate and extent of penetration of each drug into pulmonary lesions and lung tissue were estimated using nonlinear mixed-effects pharmacokinetic modeling. Our results provide the basis required to address the question of whether insufficient lesion penetration may contribute to the long treatment duration, persistence of TB disease, and continuous emergence of drug resistance.

(Part of this work was presented at the Second International Workshop on Clinical Pharmacology of Tuberculosis Drugs, San Francisco, CA, 2009.)

MATERIALS AND METHODS

All animal experiments used New Zealand White (NZW) female rabbits (weight, 2.4 to 3 kg) and were performed with the approval and oversight of the Animal Care and Use Committee of the United States National Institutes of Health (NIH), National Institute of Allergy and Infectious Diseases (NIAID). For each drug under consideration, pharmacokinetic experiments were conducted in both healthy animals and animals infected with *M. tuberculosis*. A series of four separate studies was conducted to assess the pharmacokinetics of INH, RIF, PZA, and MXF in plasma when these compounds were given alone (see Table S1 in the supplemental material). On the basis of (i) exposure seen over the dose ranges studied and (ii) human exposure at clinical doses known to be efficacious, an additional four studies were conducted to assess the pharmacokinetics of these agents in plasma, healthy lung, and *M. tuberculosis*-infected lesions when administered alone or in combination (Table 1). The latter studies were conducted in rabbits that had been infected with *M. tuberculosis* for 6 to 9 weeks prior to drug administration. Groups of *M. tuberculosis*-infected rabbits received INH or RIF alone for 8 days or a combination of INH, RIF, PZA, and MXF either as a single combined dose or as multiple combined daily doses as described in Table 1. Serial plasma, uninvolved lung tissue, and granulomas were collected in these studies.

Pharmacokinetic studies in uninfected rabbits. Healthy NZW rabbits received one single drug dose per day, orally, on either a single day or 10 to 12 sequential days, as listed in Table 1. The individual agents were

compounded as directed by the NIH Veterinary Pharmacy by grinding the drug powders (INH, PZA, MXF) with Oraplus suspending vehicle (Paddock Laboratories, Minneapolis, MN) in a mortar and pestle until dissolved or evenly suspended. An equal volume of Orasweet flavored syrup vehicle containing 1 ml raspberry flavor (LorAnn Oils Inc., Lansing, MI) was used for a final ratio of 50:49:1, as described in reference 54. RIF for intravenous (i.v.) administration (600 mg) was first dissolved in 10 ml of water for injection, prior to use in compounding. Oral doses were administered by syringe with an attached 3-in.-long piece of Tygon tubing, enabling the delivery of the drug to the back of the mouth in a restrained but awake animal, and the total volume was adjusted to account for the dead volume remaining in the syringe so that the appropriate dose was administered. Blood was sampled and collected in heparinized tubes at 0, 0.5, 1, 2, 4, 6, 8, and 24 h postdosing. Samples were processed as described in "Pharmacokinetic measurements" prior to drug level determination.

Aerosol infection and pharmacokinetic studies in infected rabbits. *M. tuberculosis* strain HN878 was maintained on Middlebrook 7H11 agar and frozen as described previously (47). For rabbit infection, the aerosol inocula were prepared by diluting frozen stocks to 1×10^6 CFU/ml in phosphate-buffered saline (PBS) and loaded into a 1-jet BANG nebulizer (CH Technologies, Westwood, NJ). The rabbits were restrained in veterinary bags with hoods, placed in exposure tubes, and exposed to the aerosol for 10 min using a CH Technologies inhalation system (Westwood, NJ) designed specifically for rabbits, followed by clean air for 10 min, before being returned to their cages. This delivered approximately 100 CFU/liter of infectious aerosol and generated 50 to 100 granulomas per rabbit lung (54). The infection was allowed to develop for 6 to 9 weeks, after which rabbits received single or multiple (5 to 8) oral doses of a mixture of INH (50 mg/kg of body weight), PZA (125 mg/kg), and MXF (25 mg/kg) and a separate dose of RIF (30 mg/kg), all prepared in the same manner as described above under "Pharmacokinetic studies in uninfected rabbits" (Table 1). Prior to euthanasia, the animals received a chest computed tomography (CT) scan to assess the extent of disease and cavity formation in the lung. Rabbits were sacrificed at various time points between 1 and 17 h following drug administration. Serial blood samples were drawn into heparinized tubes obtained from each animal at practical times between drug administration and sacrifice, in the range of 0 to 2 h postdosing. All plasma and tissue collection times were recorded.

Rabbits used in infection studies were housed in individual cages in a biosafety level 3 (BSL-3) animal facility approved for the containment of *M. tuberculosis*. Rabbits were sedated with an intramuscular injection of ketamine (25 mg/kg) plus acepromazine (0.5 mg/kg) prior to euthanasia with the Beuthanasia-D agent at 200 mg/ml (3 to 4 ml Beuthanasia-D injected i.v. through the marginal ear vein). Death was verified by the absence of breathing, absence of heartbeat, and change in mucous membrane color. All *M. tuberculosis*-infected rabbit tissues were processed in a certified BSL-3 facility until the viable organisms had been inactivated.

Necropsy and tissue dissection. Final blood samples were collected under sedation, and euthanasia procedures were immediately followed by necropsy, with organ removal being no more than 10 min after the last blood draw. The organs were removed, and the lung was weighed and dissected into lobes. The lobes were photographed, and the anatomical location, number, type, and size in the largest dimension of the lesions were recorded. Granulomas were measured with a sterile micrometer after dissection away from normal tissue. To determine drug concentrations in tissue, three to six small pieces (0.1 to 0.2 g) of grossly uninvolved lung were obtained from each animal, weighed, and snap-frozen. Lesions ranging from 1 to 6 mm in diameter were dissected from normal lung parenchyma, weighed, and cut into pieces for histology, bacterial burden determination, and drug concentration measurement. Tissue for drug distribution analysis was weighed and snap-frozen. The lesion pieces and slices of the remaining lobes and other organs were exposed to 10% neutral buffered formalin for a minimum of 24 h prior to processing for paraffin embedding. Each tissue block was cut into 5-μm consecutive sections that were then stained with standard hematoxylin and eosin and

the Ziehl-Neelsen acid-fast stain. The lesions were initially categorized into either solid, coalescing, caseous, or suppurative granulomas on the basis of gross appearance at dissection and confirmed on histological examination of stained sections. Cavities were identified by CT scans and located during dissection; they were divided into interior caseum and cavity wall as follows. The cavity was sliced open using a clean scalpel, and a sample of caseum was transferred to a clean preweighed tube. The cavity wall was dissected away from the normal lung tissue and placed on a clean petri dish; the interior caseum was scraped off the interior wall surface with a clean scalpel blade, and the wall was transferred to the storage tube for later homogenization.

Pharmacokinetic measurements. To build calibration curves, drug-naive lung and lesion tissues were obtained from infected untreated rabbits and were gamma irradiated on dry ice in a cobalt 60 3-rod irradiator in the full-power position to eliminate viable *M. tuberculosis* bacilli (3 megarads). They were kept at −20°C until they were used as naive matrix spiked with known amounts of drugs. Frozen drug-free tissue was thawed at room temperature and homogenized in PBS using a Qiagen Tissue-Lyzer. For every 0.2 g of tissue, 1 ml of PBS was added. Drug-containing plasma, lung, and lesion samples were not gamma irradiated but, rather, processed as follows. Blood samples were collected in heparinized tubes and centrifuged for 10 min at 5,000 × *g*, and plasma was stored at −80°C. Lung and lesion samples were homogenized in PBS with a Polytron PT 3000 homogenizer as described above in a BSL-3 facility biosafety cabinet. To 50 μl of either plasma or homogenized tissue, 10 μl of methanol was added. After thorough vortex mixing, 440 μl of acetonitrile was added, the mixture was vortexed again for 2 min and centrifuged at 10,000 × *g* for 10 min, and the supernatant was removed to a clean tube. Supernatants (200 μl) were transferred to 96-well plates and lyophilized. Plates were generated in triplicate, transferred out of the BSL-3 area, and stored at −20°C until reconstituted in mobile phase and analyzed.

High-pressure liquid chromatography (HPLC) coupled to tandem mass spectrometry (LC/MS/MS) analysis was performed on a Sciex Applied Biosystems API 4000 triple-quadrupole mass spectrometer coupled to a Spark Symbiosis Pharma HPLC system. Sample analysis was accepted if the concentrations in the low-level quality control samples were within ±20% of the nominal concentration and those in the mid- and high-level quality control samples were within ±15%. Gradient elution conditions with an Agilent Zorbax Phenyl column (4.6 by 75 mm; particle size, 3.5 μm) were used. Mobile phase A was 0.2% acetic acid in deionized water, and mobile phase B was 0.2% acetic acid in acetonitrile. Multiple-reaction monitoring of parent/daughter transitions in electrospray positive-ionization mode was used to track the presence of analytes. Quantitation of drug levels was performed using the transitions 138.0/121.1 for INH, 823.1/791.2 for RIF, 124.0/79.1 for PZA, and 402.2/261.2 for MXF. Mass spectrometer source conditions were optimized for each analyte. Standards, quality control samples, and blanks in matching matrix were used (drug-free plasma, healthy lung, or lesion material). Data processing was performed using Analyst software (version 1.4.2; Applied Biosystems Sciex).

Pharmacokinetic data modeling. A nonlinear mixed-effects analysis was performed by simultaneously modeling all available plasma and tissue drug concentration data for each study drug. With this population approach, the central tendency in the population, i.e., the typical value, as well as the variability, e.g., interindividual variability (IIV) and residual error, is described. The model-building process was performed in a stepwise fashion, developing first the structural plasma PK model, including variability. In a second step, a full model also describing lung and lesion penetration was developed, keeping the parameters of the plasma PK model fixed. As a last step, covariate relationships on the parameters of the lesion PKs were investigated, after which all parameters were reestimated. The likelihood ratio test (LRT) was used to evaluate statistical significance for inclusion of additional parameters in nested models, assuming that the objective function value (OFV) is χ^2 distributed; thus, a decrease in OFV of 3.84 points between hierarchical models with one parameter differing is

considered a statistical difference with a 5% significance level. Goodness-of-fit plots computed in the Xpose (version 4.0) program (25) were also used to guide model selection.

(i) Plasma PK model. One- and two-compartment models with a first-order elimination, parameterized in terms of oral clearance (CL), oral volume of distribution (V), intercompartmental clearance (Q), and peripheral volume of distribution (V_2), were fitted to the data. All doses were given per kg of body weight and were modeled as such, given the narrow weight range in this experimental animal population. Several different models were tried for the absorption profile of the drugs: a first-order model, a combined first- and zero-order model with an estimated duration of zero-order input, a transit compartment model with a fixed or estimated number of compartments (50), and the Weibull absorption model (45). The potential impact of drug-drug interactions (DDIs) was explored by examining changes in the relative bioavailability, clearance, and oral volume of distribution parameters with multiple-drug studies or multiple-dosing studies. Interindividual variability was allowed on all plasma PK parameters and assumed to be lognormally distributed. A full covariance-variance structure was initially estimated with reductions allowed on the basis of the magnitude of estimates and the LRT.

(ii) Tissue penetration model. The lung and lesion drug penetration was described using effect compartment models similar to those of Gobburu et al. (19) with the following equations:

$$dC_{\text{lung}}/dt = k_{\text{pl-lung}} \cdot \left(PC_{\text{lung}} \cdot \frac{A_{\text{plasma}}}{V_{\text{plasma}}} - C_{\text{lung}} \right)$$
$$dC_{\text{lesion}}/dt = k_{\text{pl-lesion}} \cdot \left(PC_{\text{lesion}} \cdot \frac{A_{\text{plasma}}}{V_{\text{plasma}}} - C_{\text{lesion}} \right) \quad (1)$$

where C is concentration, $k_{\text{pl-lung}}$ and $k_{\text{pl-lesion}}$ are the time rate constants for the transfer of drug from the plasma to lung or lesion, in h^{-1}, PC_{lung} and PC_{lesion} are the penetration coefficients between plasma and lung or lesion, and $A_{\text{plasma}}/V_{\text{plasma}}$ is the concentration of drug predicted in the plasma compartment at time t, with A_{plasma} being the amount of drug in plasma and V_{plasma} the apparent volume of the plasma compartment. Interindividual variability was investigated on the parameters belonging to the tissue penetration model, but as only observation samples at the time of necropsy were available from each individual for these tissue compartments, separation of interlesion variability and residual error was not possible.

(iii) Residual error model. All data were analyzed in the logarithmic domain to increase the stability of the model estimation process and to reduce run times. Several models describing the residual variability were investigated: additive and proportional error models and a slope-intercept model. Different residual errors were estimated for plasma, lung, and lesion. As replicates were available for some observations and any errors made in the sampling procedure would affect all concentration measurements in this sample, these replicates were modeled as having one common and one separate error term.

(iv) Covariate model. Size and type of lesion were investigated as covariates on rate and extent of drug penetration into lesions (i.e., $k_{\text{pl-lesion}}$ and PC_{lesion}). Size of lesion was reported in the closest half mm of diameter with a median of 2 mm. Size of lesion was treated as continuous, and the correlation to penetration was assessed using a power model centered on the median lesion size of 2 mm as described by the following equation:

$$P = \theta_p \cdot \left(\frac{\text{size}_i}{2} \right)^{\theta_{\text{size}}} \quad (2)$$

where θ_p is the typical value of parameter P ($k_{\text{pl-lesion}}$ or PC_{lesion}) for lesions with a size of 2 mm (median of the lesion population), and θ_{size} is the rate of change of $k_{\text{pl-lesion}}/PC_{\text{lesion}}$ for lesion size. Missing size measurements were assumed to be of median size. The impact of lesion type was also assessed in a binary fashion:

$$P = \theta_p \cdot \theta_{\text{type}}^{1 - \text{type}} \quad (3)$$

where θ_p is the typical value of the parameter P ($k_{\text{pl-lesion}}$ or PC_{lesion}) for lesions of type 1 and θ_{type} is the fractional change in P for lesions of type 0.

The different lesion types, solid, coalescing, caseous, and suppurative, were investigated one at a time by being coded as 0, while all other lesion types were imputed as 1. If one parameter showed a statistical significance with several lesion types, a full categorical covariate model where the value of the parameter P is different for each of the lesion types was investigated. In this last approach, all types not classified as solid, coalescing, caseous, or suppurative were coded as solid lesions, i.e., as belonging to the largest group, as these lesions were considered small and homogeneous with a granular interior, similar to the larger solid lesions.

The importance of retaining a covariate in the model was judged using the LRT, but also on the basis of an empirical clinical irrelevance criterion as proposed by Tunblad et al. (53), i.e., the magnitude of reduction in interindividual variability and residual error and the fractional change in the parameter value between the smallest and the largest values of the covariate distribution (53).

(v) Model evaluation. Percentile confidence intervals for all parameters in the final model were computed from the estimation of 500 resampled nonparametric bootstrap data sets. Visual predictive checks were performed to evaluate the simulation properties of the final model. The 90% prediction interval was computed for simulations of 10,000 individuals. If the model adequately describes the data, 90% of the observed data should be evenly distributed within the prediction interval. For each individual, the predicted area under the concentration-time curve (AUC) and maximum concentration (C_{max}) in plasma, lung, and lesion were also computed using NONMEM.

(vi) Software. Data were analyzed using the first-order conditional estimation method as implemented in the software NONMEM, version 7 (ICON Development Solutions). Graphical, statistical, and exploratory analyses were conducted using the R package (version 2.11.1), while Xpose (version 4.0) was used for data set checkout and graphical evaluations of the modeling output (25). Nonparametric bootstrap and visual predictive check were performed using PsN software (version 3.2.12) (33, 34), and scripts were created using R.

RESULTS

Determination of plasma and tissue concentrations of INH, RIF, PZA, and MXF in rabbits. To select an appropriate dose that approximated human exposure (1, 4, 38, 52), we first determined the plasma concentration-time profiles of INH, RIF, PZA, and MXF in uninfected rabbits following administration of one to three different doses, either as single doses or after attaining steady state. Figure 1 shows the profile of each drug at the indicated doses. The pharmacokinetics of INH and RIF were linear within the range of doses tested. Contrary to reports of RIF inducing its own metabolism *in vitro* and in some TB patient populations (36), our PK data in uninfected rabbits revealed steady-state RIF exposure about 5-fold higher than single-dose exposure at both doses tested. It should be noted that reduced steady-state clearance has also been observed in some patient populations (58). We observed overproportional exposure of MXF at 50 and 100 mg/kg compared to 20 mg/kg. On the basis of calculated AUC and C_{max} values and given the ranges of linearity observed, the following doses were adopted for all further studies in infected rabbits, in order to approximately reproduce human exposure at clinically used doses: INH, 30 mg/kg (fast acetylator phenotype) or 50 mg/kg (slow acetylator phenotype); RIF, 24 or 30 mg/kg; PZA, 125 mg/kg; and MXF, 25 mg/kg. The PZA dose of 125 mg/kg provides peak plasma concentrations within the range of those observed in human (20 to 60 μg/ml) but a lower AUC due to the shorter half-life seen in the rabbit. However, this was the highest dose approved by the IACUC of NIH-NIAID, which dictated our dose selection.

Rabbits infected by aerosol were housed for 6 to 9 weeks to ensure adequate time for well-structured granulomas to develop
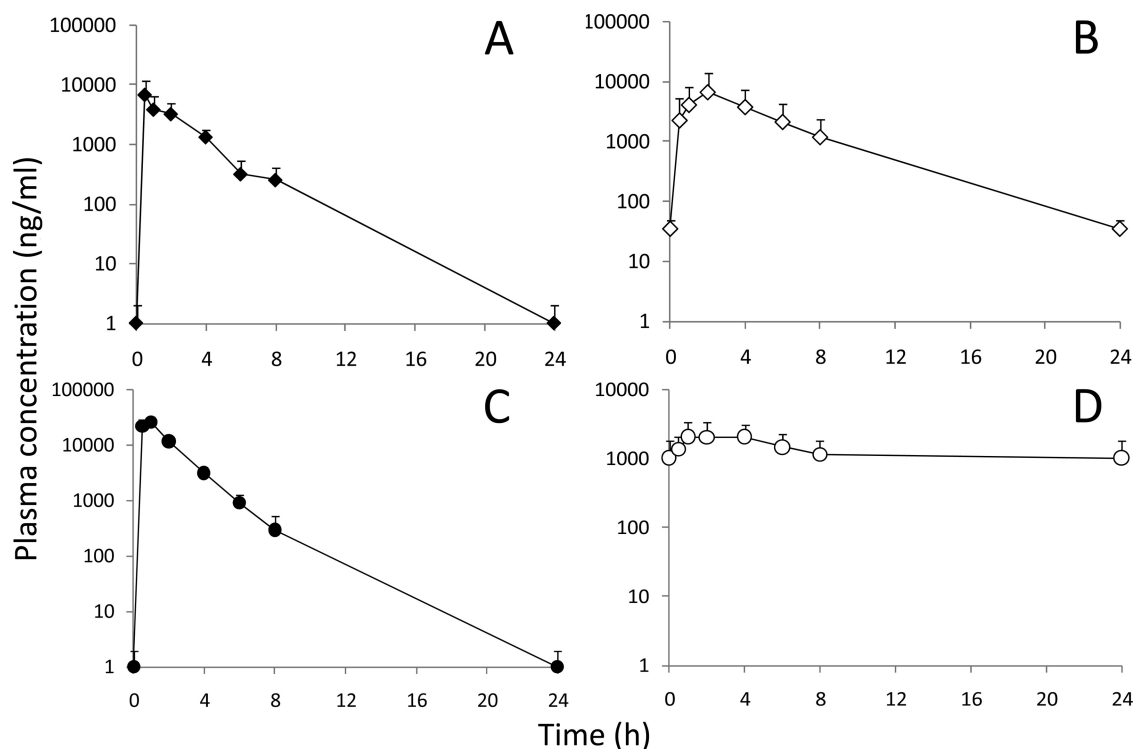
FIG 1 Plasma concentration-time profiles of healthy rabbits following multiple (10 to 12) daily doses. (A) INH, 30 mg/kg; (B) RIF, 24 mg/kg; (C) PZA, 125 mg/kg; (D) MXF, 20 mg/kg. Average plasma concentrations with standard deviations ($n = 4$) are indicated.

before receiving all four drugs simultaneously in a single dose at predefined time points prior to necropsy. Tissue samples were harvested, and individual lesions, as well as apparently normal lung samples, were segmented for drug level determination as well as histopathology. For this initial single-dose study, 13 rabbits were sacrificed and lung/lesion samples were collected at various times between 0.5 and 7 h (Table 1). A total number of 44 uninvolved lung samples and 46 solid granulomas were collected in this study. Noncompartmental analysis (NCA) was applied to this data set, and the total AUC for each type of lesion was calculated to allow comparison of absolute concentration ratios among lesions, healthy lung, and plasma. AUC ratios generated in this analysis showed that RIF and MXF accumulate into uninvolved lung tissue to a greater extent than INH and that PZA distributes poorly from plasma to lung tissue. In contrast to the drug levels in healthy lungs, drug concentrations within lesions were all significantly lower than plasma concentrations, with the single exception of MXF (Fig. 2, noncompartmental analysis). Only MXF accumulated in lesional material, with a lesion-to-plasma AUC ratio greater than 7. This is in agreement with the spatial distribution of MXF in rabbit lung and granulomas observed by imaging mass spectrometry (46). The methods used in this work have provided total drug concentrations rather than free fractions (i.e., non-protein bound). However, none of the study drugs is highly bound to plasma proteins, with negligible binding for INH and PZA, less than 50% for MXF, and about 80% for RIF.

Determination of plasma and lesional concentrations at steady state. We examined plasma and tissue samples from three other groups of infected animals. The first two groups of four animals were dosed with either INH or RIF alone for 8 days, before

receiving a final dose at a predetermined time prior to sacrifice. In the third group of 12 animals, all four drugs were administered daily for 5 to 6 days. There were no significant quantitative differences in the plasma and lesional drug levels between animals at steady state and animals that had received only a single dose (data not shown). Therefore, we analyzed the data generated from all
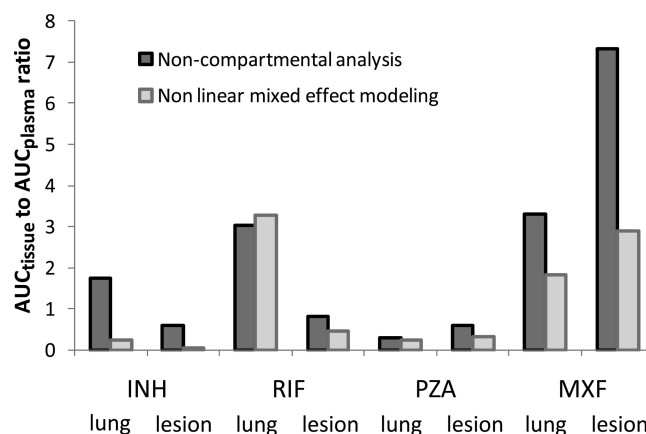

FIG 2 Histograms of AUC ratios between tissue (lung or lesion) and plasma for each of the four study drugs. Predicted AUC ratios from the population analysis (PopPK) are compared with those computed using noncompartmental analysis (NCA) of data from the single-dose study with all four drugs administered together (dark gray bars). Individual AUC ratios from the population analysis were obtained from the effect compartment population PK model, based on all four lesion PK studies described in this work (light gray bars).
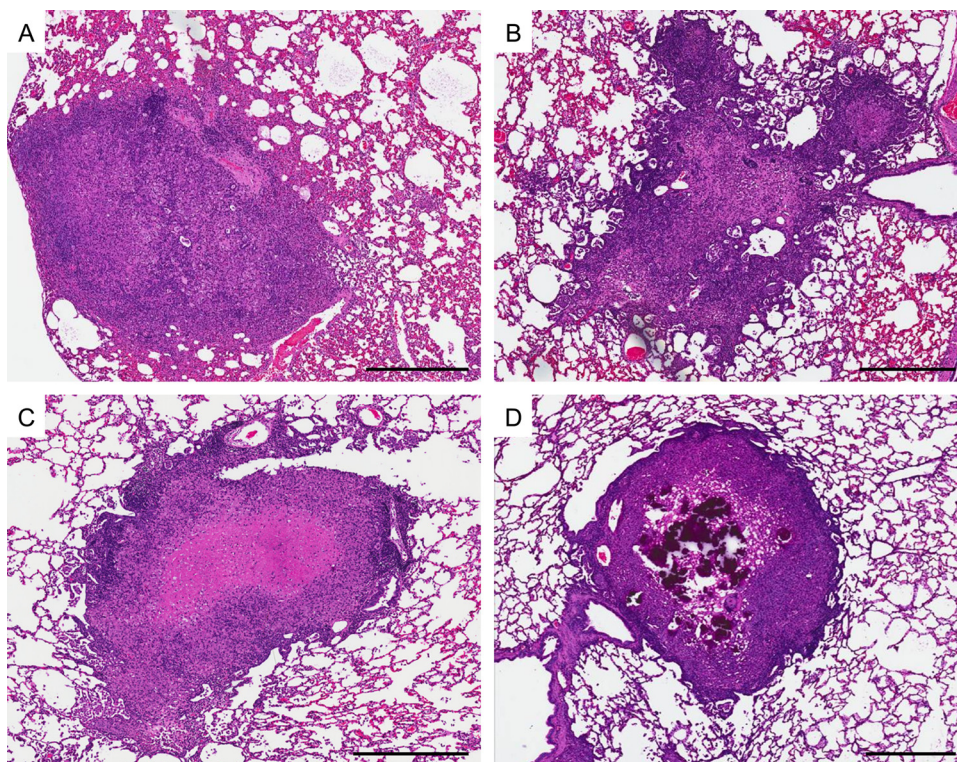
FIG 3 Composite photo of granuloma types sampled in this study. (A) Nonnecrotizing, predominantly cellular granuloma, with central epithelioid macrophages and no necrosis visible at dissection; cellular granulomas were typically ≤2 mm in diameter; (B) three or four coalescing nonnecrotizing granulomas that could not be divided into separate lesions during dissection; (C) necrotizing granuloma with central acellular region visible at dissection; (D) cavitating necrotic lesion which has become suppurative and macroscopically demonstrates a semiliquid core that oozes from the lesion during dissection. Histologically, the section shows infiltrating neutrophils and macrophages in the suppurative caseum. Bars, 500 μm.

four tissue distribution studies together, using an effect compartment and a nonlinear mixed-effects modeling framework. Figure 2 shows that the same trend in lung and lesion partitioning for each of the study drugs was observed, whether NCA or mixed-effects modeling was used. However, the numerical values of tissue-to-plasma ratios were overall lower when all data sets were analyzed using the population PKs approach (compare NCA with nonlinear mixed-effects modeling). Collectively, these observations indicate that similar results of tissue penetration were obtained in independent single-dose and steady-state studies and that both NCA and population PK modeling concluded that MXF has the highest distribution from plasma into rabbit lesions.

In studies where uninvolved and diseased lung tissues were collected, the size and type of each granuloma were recorded, in order to determine any relationship between lesion size and type and drug penetration. Essentially, four different types of granulomas could be differentiated on the basis of visual inspection at dissection and subsequent histological review: solid, coalescing, caseous, and suppurative granulomas. Representative examples of the types of granulomatous lesions sampled in this work are presented in Fig. 3. In addition, three cavities were identified in one of the animals during CT scanning (L. E. Via et al., unpublished data), collected during necropsy, which took place at 5 h postdosage, and separated into cavity caseum and cavity wall for drug quantification. We observed that MXF again had the highest distribution into cavity caseum and cavity wall, with tissue-to-plasma ratios of 9 and 16, respectively. RIF distributed equally

between caseum and wall, with a tissue-to-plasma ratio of approximately 3, and INH appeared to penetrate caseum better than the fibrotic wall, with tissue-to-plasma ratios of 2 and 0.5, respectively. No PZA could be detected in caseum, while concentrations measured in the cavity wall were similar to those concomitantly observed in plasma. Given the limited number of cavity samples, which, in addition, originated from one rabbit only, these data were not included in the modeling and should be interpreted with caution.

Pharmacokinetic modeling of drug concentrations in plasma. A schematic representation of the population pharmacokinetic models developed for RIF, MXF, PZA, and INH is shown in Fig. 4, and parameter estimates are given in Table 2. All drugs were described using a two-compartment model with first-order absorption and first-order elimination. A two-compartment transit absorption model was used to describe all drugs' absorption, apart from that of PZA, for which only one absorption compartment was used. All final models had a reduced variance-covariance structure. DDIs were found for RIF when comparing single-drug with combination data. Given the known DDIs between RIF and other antituberculosis drugs (41), we fixed the bioavailability to 1 in the model when RIF was given in combination and allowed it to vary when RIF was administered as single drug. Proportional error models adjusted for replicates were found to best describe the residual error of the observations of the four drugs. This model consisted of one proportional error term that is unique for each observation and one proportional error
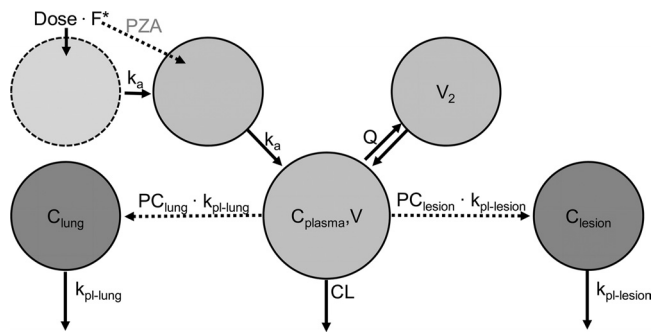
FIG 4 Schematic picture describing the models for plasma pharmacokinetics and tissue penetration. The model for PZA included one absorption compartment. k_a, absorption rate constant; V, oral volume of distribution; CL, clearance; V_2, peripheral volume of distribution; Q, intercompartmental clearance; F, relative bioavailability for combination therapy; PC, penetration coefficient from plasma into lung or lesion; $k_{pl-lung/lesion}$, distribution rate constant. Bioavailability (F) was fixed to 1 for all drugs but RIF, where the relative F was estimated for all single-dose studies and fixed to 1 for combination-therapy studies.

FIG 5 Observed plasma concentrations of INH, RIF, PZA, and MXF versus individual model-predicted concentrations. Solid line, line of identity.

term that is the same for replicates. These two terms were estimated to have different variances. Additionally, values below the limit of quantification but above the limit of detection were kept in the data set but were allowed to have a higher residual error than observations above the limit of quantification. All previously published analyses of plasma PKs of INH, PZA, and MXF in rabbits show biphasic kinetics after rich sampling schedules (7, 8, 17, 57). Though a direct comparison of population estimates is difficult as these data sets were modeled using noncompartmental analysis methods, the predicted and previously reported C_{max}s after an equivalent dose of each drug were similar, as were the predicted and previously observed times to C_{max} (T_{max}). The final models could adequately describe the plasma PKs of the four drugs. The acceptability of the model fit is interpreted from the randomness and closeness of the data scattered around the line of identity throughout the data range (44). In the plots showing predicted versus observed concentrations (Fig. 5), the observed data were evenly scattered around the line of identity, with no trends of deviation from the line, indicating the absence of bias. No such
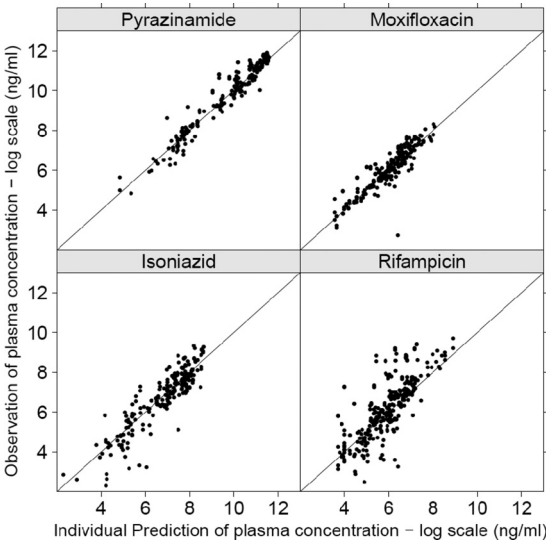
trend was observed in any of the goodness-of-fit graphs investigated.

Pharmacokinetic modeling of drug concentrations in tissue and lesions. The parameters of the plasma PKs were fixed while investigating the tissue penetration model, assuming that plasma PKs are unaffected by lung and lesion PKs. The initial lung and lesion PK models included interindividual variability (IIV) on all parameters belonging to the lung and lesion models with correlations. These models were later reduced using the same approach used for the plasma PK models. Table 2 summarizes the characteristics of the penetration into tissue, where the equilibrium rates are represented as equilibrium half-lives. The extent of penetration into lesions was highest for MXF and lowest for INH, as judged by the estimated penetration coefficients (PCs). For RIF, penetration into healthy lung tissue was better than into lesions. The variability of the extent of penetration was higher in lesions than in lung for all drugs. The typical values of the PCs and the

TABLE 2 Parameter estimates of the final model for INH, RIF, PZA, and MXF, reported as typical value and interindividual variability expressed as coefficient of variance[a]

Parameter	INH Typical value (% RSE)	INH % CV (% RSE)	RIF Typical value (% RSE)	RIF % CV (% RSE)	PZA Typical value (% RSE)	PZA % CV (% RSE)	MXF Typical value (% RSE)	MXF % CV (% RSE)
k_a (h^{-1})	0.884 (7.8)	5.73 (39)	3.16 (18)		0.639 (23)	38.1 (77)	1.68 (10)	25.4 (55)
CL (liter/h kg)	2.85 (8.3)	29.4 (22)	1.48 (11)	1.58 (23)	0.750 (14)	75.0 (11)	3.77 (17)	99.9 (39)
V (liter/kg)	0.08 (-)		22.5 (18)	49.8 (60)	0.371 (56)	58.5 (57)	1.95 (29)	261 (22)
Q (liter/h kg)	2.02 (30)	156 (110)	0.325 (17)	10.7 (4.6)	0.273 (23)	48.0 (23)	16.1 (15)	66.7 (38)
V_2 (liter/kg)	27.5 (12)		0.197 (21)		3.98 (37)	86.7 (210)	30.2 (22)	72.2 (44)
F comb.			0.460 (13)	73.0 (40)				
$t_{pl-lung}$ (min)	20 (380)	5.59 (610)	1 (—)	102 (2370)	63 (87)		2 (41)	775 (265)
PC$_{lung}$	0.254 (8.5)	6.07 (35)	3.32 (17)	39.7 (60)	0.271 (18)	56.0 (42)	1.85 (11)	44.4 (50)
$t_{pl-lesion}$ (min)	1 (—)	11.2 (3500)	1 (—)	97.6 (1290)	54 (68)	415 (150)	23 (35)	
PC$_{lesion}$	0.0660 (17)	36.7 (60)	0.456 (21)	66.5 (51)	0.334 (13)	59.7 (165)	3.09 (18)	81.1 (39)

[a] Uncertainty of estimate, i.e., relative standard error (RSE; in percent) calculated on the basis of results for 200 nonparametric bootstrap samples, is given in parentheses after the estimate. Parameters where no uncertainty is given were fixed in the estimation. CV, coefficient of variance; k_a, absorption rate constant; V, oral volume of distribution; CL, clearance; V_2, peripheral volume of distribution; Q, intercompartment clearance; F comb., relative bioavailability for combination therapy; PC$_x$, penetration coefficient; and t_{pl-x}, equilibration half-life derived from $\ln(2)/k_{pl-x}$, where k_{pl-x} is the time rate constant to lung or lesion tissue.

TABLE 3 Average predictions of AUC, C_{max}, and half-life for each study drug in plasma, uninvolved lung, and lesion[a]

Drug	No. of animals	Plasma			Uninvolved lung			Lesion		
		C_{max} (ng/ml)	AUC (ng · h/ml)	$t_{1/2}$ (h)	C_{max} (ng/g)	AUC (ng · h/g)	$t_{1/2}$ (h)	C_{max} (ng/g)	AUC (ng · h/g)	$t_{1/2}$ (h)
INH	16	2,790 (1,437)	15,048 (4,921)	0.68 (0.24)	200 (102)	3,826 (1,258)	0.18 (0.06)	189 (104)	1,024 (416)	0.05 (0.02)
RIF	30	1,121 (1,543)	14,785 (11,812)	1.18 (0.49)	1,163 (2,979)	54,798 (54,798)	4.38 (2.70)	712 (1,369)	8,993 (12,358)	0.67 (0.59)
PZA	28	57,360 (27,728)	208,801 (126,077)	7.17 (5.96)	10,134 (5,438)	54,815 (32,729)	2.07 (1.69)	10,257 (5,574)	68,106 (50,272)	4.13 (6.87)
MXF	26	711 (278)	5,896 (3,099)	0.41 (0.34)	2,457 (2,325)	12,081 (7,697)	0.89 (0.82)	2,485 (2,326)	25,282 (25,754)	1.82 (2.37)

[a] Data are mean (SD). C_{max}, peak plasma or tissue concentration; AUC, area under the concentration-time curve; $t_{1/2}$, elimination half-life.

associated variability parameter were estimated with a reasonable uncertainty. The rate of penetration into tissue was fast for all drugs, with PZA having the longest equilibration half-life of 1 h, equivalent to about 3 h to reach equilibrium concentrations in tissue. Penetration into lesions by INH and into both lesion and lung by RIF was instantaneous, and these rates were fixed to the equivalent of an equilibration half-life of about a minute in order to stabilize parameter estimation. For RIF and PZA, the estimated rates of penetration into lung and lesion were similar, while INH was slower to equilibrate into lung than into lesion, and the opposite was true for MXF. Variability of the rates was high and was higher for lesions than for lung for most drugs. The PCs were reasonably well estimated in regard to the typical population estimates, while the variability of the rate estimates was highly uncertain in most cases.

The estimated PC describes the extent of distribution of drug into a tissue taking the distribution delay into account. Ratios of AUC or C_{max} are commonly used as the predictor of the difference in drug concentration among various tissues over time. However, these ratios do not take the equilibration rate into account. For agents with a penetration half-life of less than an hour, the effect of the distribution delay on a 24-h AUC is minimal. This is shown by the values for PC being similar to the AUC_{tissue}-to-AUC_{plasma} ratio (Table 2; see also Fig. 8) for all four compounds. With a nearly instantaneous equilibration, the PC is also similar to the C_{max} ratio between tissue and plasma. However, compounds with longer equilibration half-lives will show a larger discrepancy between the C_{max} ratio and the value for penetration, as the time for peak concentration in the tissue is delayed. Hence, C_{max} ratios are more sensitive to the rate of equilibration than AUC ratios. In this study, all drugs were estimated to have high equilibration rates, with the equilibration half-life being shorter than an hour in any tissue. As a consequence, the C_{max} (results not shown) and AUC ratios are similar to each other as well as to the estimated PCs (Table 2; see Fig. 8).

From the model, we determined primary individual (i) parameters, i.e., CL_i, V_i, Q_i, $V_{2,i}$, $k_{pl\text{-}lung,i}$, $PC_{lung,i}$, $k_{pl\text{-}lesion,i}$, and $PC_{lesion,i}$ for each animal. These individual parameters were then used to calculate secondary parameters of AUC, C_{max}, and half-life for each animal. Average predictions of AUC, C_{max}, and half-life for each drug in each tissue type are presented in Table 3. The interindividual and interlesion variabilities are high, as indicated by the high standard deviations.

Association of lesion type with drug penetration ability of each agent. Investigation of covariate relationships on $k_{pl\text{-}lesion}$ (rate) or PC_{lesion} (extent) was performed once the structural model was finalized. No covariate relationships were significant according to the likelihood ratio test. This is a reliable conclusion, as part of the model was fixed throughout the search and the observed drop in objective function value with added covariate

relationships represented an overestimate of the drop expected, had all parameters in the model been estimated. The final individual predictions of lung and lesion concentrations are shown in Fig. 6, with the actual observed lung and lesion concentrations included as open circles. As shown in the figure, the variability in lesion concentrations was considerable for all compounds, which limits the ability to detect a covariate relationship across different lesion types. There were no numerical differences across lesion type for RIF and INH. For PZA and MXF, there were modest numerical differences in the covariates for the less solid (suppurative and coalescing) lesions compared with the caseous and solid lesion types. As mentioned previously, the penetration rate was estimated to be different between lung and lesion for MXF and INH. Even though the difference between lung and lesion equilibrium would be approximately 1 h, this does not seem to have a large impact on the predictions, as judged by Fig. 6. The highest variability of rate of penetration was observed for PZA into lesion and MXF into lung. The variety of shapes seen in Fig. 6 is a result of this high variability.

The visual predictive checks for the final models are shown in Fig. 7. The large interindividual variability in the plasma PK model is the cause for the wide 90% prediction interval of the data; however, the main trend in the data for plasma, lung, and lesion is well captured by the model.

Figure 8 shows the range of calculated AUC ratios based on the individual predictions of AUC in plasma, healthy lung, and lesion tissue. The median in each bar is the same value reported in Fig. 2 (nonlinear mixed-effects modeling). The size of the boxes of the AUC ratios is an indication of how correlated an individual plasma AUC is to its corresponding individual tissue AUCs and is related to the unexplained variability in the model. For all drugs except PZA, the variability of the ratios was higher for lesion than for lung, likely owing to the more homogeneous nature and consistent blood supply of healthy than diseased lung tissue. The very short box observed in Fig. 2 for the INH lung-to-plasma ratio indicates that all individual ratios between lung and plasma were almost identical. In relative values, an individual with high INH plasma exposure always had high INH lung exposure and vice versa. Figure 8 also shows the consistency with which tissue ratios are predicted. For each drug in each tissue type, the individual values of tissue-to-plasma ratios clustered either above or below the line of equal partitioning, with the exception of two data points in the RIF lesion-to-plasma data set. None of the gray boxes or interquartile ranges of the predicted ratios crossed the line of even distribution.

DISCUSSION

Plasma and tissue PKs of INH, RIF, PZA, and MXF in *M. tuberculosis*-infected rabbits were described using a nonlinear mixed-effects modeling (population) approach. To our knowl-
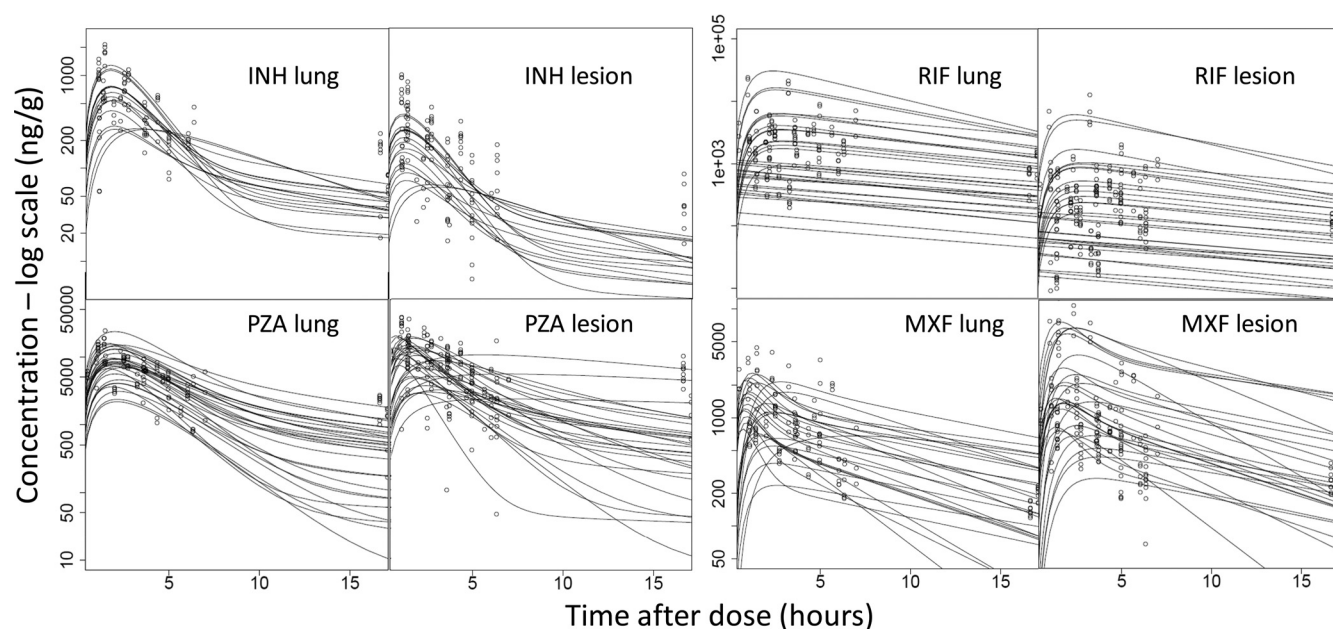
FIG 6 Predicted concentration-time profiles for each individual animal are shown as solid lines. Observed concentrations are indicated by open circles. Data are shown for INH, RIF, PZA, and MXF in lung tissue and lesions.

edge, this is the first time that both the rate and extent of drug distribution into pulmonary TB lesions have successfully been determined. Our results show that the three major first-line agents used against TB reach lesion concentrations that are lower than those found in plasma, with INH having the lowest coefficient of penetration in both healthy lung and lesions. In contrast, MXF (one of the most effective second-line agents) displayed the highest distribution from plasma to lesion. These conclusions were reached using both noncompartmental and model-based PK analysis methodologies (Fig. 2).

In lesion PK studies reported here, INH, RIF, and MXF doses were chosen to approximate human exposure seen at clinically used doses. Under these conditions, the average AUC_{lesion}/MIC for MXF is about 100, above the free AUC/MIC of 53 associated with suppression of the *M. tuberculosis* drug-resistant mutant

population in the hollow-fiber model (22). In general, AUC/MIC breakpoints vary largely depending on the pathogen and microbiological readout (static effect, cidal effects of various magnitudes, mutant prevention). For MXF, AUC/MIC breakpoints ranging from 30 to 100 have been shown to produce similar kill effects against different pathogens *in vitro* (18, 31, 42), whereas the AUC/MIC associated with comparable *M. tuberculosis* kill is unknown. Despite the large variability observed in our study and the lack of comparable *in vitro* data of AUC/MIC breakpoints in the literature, MXF exposure in TB lesions appears to be adequate to achieve sustained killing. The INH AUC_{lesion}/MIC, on the other hand, is relatively low at 17, assuming an MIC of 0.06 μg/ml. For RIF, the calculated AUC_{lesion}/MIC is about 90 with an MIC of 0.1 μg/ml. Again, caution should be exercised when comparing these values with numbers published for other infectious diseases, given
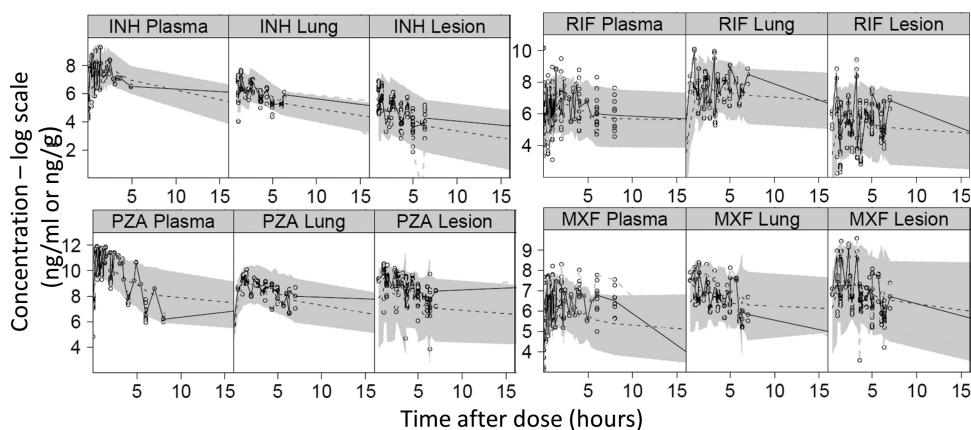

FIG 7 Visual predictive check showing the predicted main trend (dashed lines) and 90% prediction interval (shaded areas) of plasma, lung, and lesion concentrations for INH at 50 mg/kg, MXF at 25 mg/kg, PZA at 125 mg/kg, and RIF at 30 mg/kg. Actual observations at the relevant doses are overlaid (open circles) and connected with a solid line.
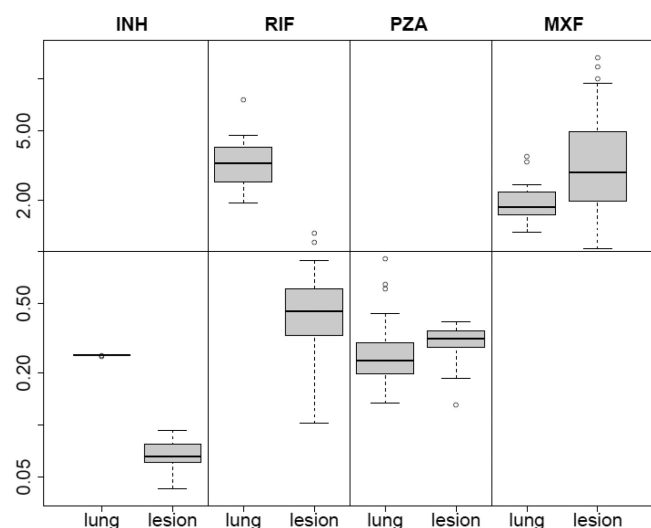
FIG 8 Box plots of the ratios of individually predicted AUCs in lung and lesion tissue relative to plasma AUC for each drug. The box width is the interquartile range, with the horizontal line marking the median value. The whiskers indicate the maximum/minimum of ratios within 1.5 times the upper/lower quartiles. Observed data points falling outside this range are represented by open circles.

the large variability seen in drug concentrations within lesions (Table 3 and Fig. 6).

Though the biological relevance of protein binding remains somewhat controversial, binding to macromolecules present in lung and lesions might be quite different from plasma protein binding, which is low to moderate for the 4 study drugs. Conforming to the common belief that free concentrations at the site of action are more appropriate PK input values for PK-pharmacodynamic (PD) analysis (35, 40), additional studies might be required to assess whether these drugs reach their site of action in sufficient free concentrations over time. More critical than correction for protein binding is the choice of MIC values in calculating PK-PD parameters. The use of the MIC against extracellular replicating bacilli determined in vitro is likely an optimistic oversimplification. It is generally recognized that various bacterial subpopulations coexist in M. tuberculosis-infected lung and that these subpopulations can exhibit phenotypic tolerance to any single drug (56). The model of Mitchison (37) and Mitchison and Coates (39) is often adopted to describe these populations and their respective drug susceptibilities, distinguishing actively growing M. tuberculosis bacteria mostly killed by INH, semidormant organisms with spurts of metabolism preferentially killed by RIF, intracellular bacilli present in the acidic phagolysosome of macrophages mainly susceptible to PZA, and dormant persisters found in hypoxic microenvironments with much reduced sensitivity to most anti-TB drugs (59, 60; our unpublished data). In this context, further work is required to determine whether each of these drugs is able to reach its respective target M. tuberculosis subpopulation in adequate concentrations for a reasonable fraction of the dosing interval. Our RIF results complement work described in a recent publication by Goutelle et al. that estimated the pulmonary permeation of a standard dose of RIF in healthy volunteers (20). RIF epithelial lining fluid (ELF)-to-plasma ratios derived from bronchoalveolar lavage fluid drug levels were in the same range as the permeation values determined here for RIF in

rabbits with TB lesions. These results were modeled to estimate the AUC_{tissue} of RIF in human subjects and showed that a large percentage of the population would be expected to have inadequate tissue concentrations of RIF with the standard dose of 600 mg. Similar to our results, these indicate that the lower-permeation drugs may need greater doses to achieve an adequate exposure at the site of action to effectively eliminate M. tuberculosis bacilli.

The PK models developed in this work could nicely describe the main trend seen in plasma concentrations (Fig. 5) and also reasonably captured the variability present in the plasma and lesion data sets (Fig. 6). In terms of extent of distribution from plasma to lesion, the four drugs ranked as follows: MXF > RIF > PZA > INH. All study drugs distributed rapidly into the relatively small lesions analyzed here. No accumulation was observed when comparing lesion concentrations after single-dose administration with those observed at steady state. Hence, these drugs appear to be "fast in, fast out" molecules with no residing concentrations after administration of drug is stopped.

Standard methods commonly use drug concentrations in plasma or organ homogenates to determine the PK-PD indices of antibiotics (2). Our data and modeling results indicate that drug concentrations in either plasma or lung homogenates are not a suitable surrogate for drug concentrations at the site of infection, since (i) none of the study drugs displayed a lesion-to-plasma AUC ratio close to 1 and (ii) lung-to-lesion ratios followed different trends for each drug (Fig. 8). This is particularly clear for INH and RIF, where the normal lung exposure ratio greatly exceeds the normal lesion exposure ratio. Accordingly, Mouton et al. have also highlighted that using concentrations in uninfected tissue homogenates alone to determine the exposure-response relationship is a misguided approach (40). Our results will enable the integration of lesion-specific PK-PD indices in clinical trial simulations to identify optimal doses (24), as well as in PK-PD hollow-fiber studies to calculate M. tuberculosis susceptibility breakpoints (21).

Comparing published numbers of ELF-to-plasma ratios with the lesion PCs calculated in this study suggests that the predictive value of the ELF-to-plasma ratio for assessing the ability of drugs to penetrate pulmonary TB lesions should be evaluated on a case-by-case basis. Overall, the estimated PC_{lesion} values for RIF and MXF followed the same trend as the PCs reported for ELF in clinical studies (51, 62), while the reported penetration of INH and PZA in ELF (10, 11, 43) is quite different from the corresponding PC_{lesion} obtained in this study.

Finally, our rabbit data are in reasonable agreement with early results from clinical studies where RIF and INH levels were measured in pulmonary TB lesions of resected human tissue (30). Following the analysis of tissue samples from several hundred TB patients, Kislitsyna and colleagues reported tissue-to-blood ratios of 8 to 22% for RIF and 4 to 42% for INH, observed between 2 and 5 h after drug administration (29). Given the marked differences in study design and readouts used for drug measurements, one cannot draw strict quantitative comparisons. However, it appears that the rabbit model is an adequate tool for preliminary evaluation of drug distribution into TB lung tissue and lesions.

There are limitations to our study that must be kept in mind. While the rabbit model presents many of the immunopathological features seen in clinical TB disease (13), rabbit nodules found at 6 to 8 weeks postinfection generally remain much less differentiated than human lesions at the time of diagnosis. In this study,

the size distribution was relatively narrow. Features typically seen in active disease, such as fibrosis and cavitation, were not present in these animals. Attempts to correlate granuloma type (solid, coalescing, caseous, and suppurative) with the rate and extent of drug penetration did not provide statistically significant relationships. Larger numbers of more differentiated lesions are likely required to power the covariate analysis. Additional drugs with different physicochemical properties, such as higher log P values and greater protein binding, are also needed to more comprehensively test the hypothesis that animal models exhibiting more diverse lesion types add value to the study of infection site pharmacodynamics. Most importantly, the method used here for measuring drug concentrations involves tissue homogenization, causing the loss of spatial resolution and information on relative distribution in different lesion compartments. We have indeed shown, using mass spectrometry imaging, that the two-dimensional distribution of MXF in rabbit necrotic granulomas is not homogeneous, with areas of high concentrations in the peripheral cellular layers relative to the necrotic core (46). Despite these limitations, we see a clear trend pointing to very different relative exposure of each of the four study drugs in diseased tissue relative to plasma. We also observe variability in the penetration of a given drug into different lesions of the same individual, which is reminiscent of antibiotic penetration into abscess and abscess fluid (49, 55).

The high variability in the data and model predictions limits the extent to which we can use these models to extrapolate and link our results to the expected behavior of these drugs in human subjects. At present, the models describe the current experiments well but will need further refinement to explore the influence of lesion covariates on understanding differences in tissue permeation. To overcome these limitations and validate the rabbit model for drug penetration studies, a multicenter clinical protocol with TB patients undergoing lung resection is currently under enrollment (NCT00816426 at www.clintrials.gov). The objective is to evaluate the penetration of RIF, INH, PZA, MXF, and kanamycin in sputum and pulmonary lesion compartments, using modern analytical, imaging, and modeling methods.

M. tuberculosis bacilli are thought to be present in different microenvironments, which in turn significantly affect their metabolic state, making them more or less susceptible to INH, RIF, and PZA (37). Further *in vivo* PK-PD studies can now be designed to characterize and localize these bacterial populations in relation to drug levels achieved locally in lesions and lesion compartments. Collectively, our results enable the integration of lesion-specific PK-PD indices in clinical trial simulations and open the door for potentially more predictive *in vitro* PK-PD studies with *M. tuberculosis*.

ACKNOWLEDGMENTS

REFERENCES

1. Acocella G. 1978. Clinical pharmacokinetics of rifampicin. Clin. Pharmacokinet. 3:108–127.
2. Barbour A, Scaglione F, Derendorf H. 2010. Class-dependent relevance of tissue distribution in the interpretation of anti-infective pharmacokinetic/pharmacodynamic indices. Int. J. Antimicrob. Agents 35:431–438.
3. Barclay WR, Ebert RH, Le Roy GV, Manthei RW, Roth LJ. 1953. Distribution and excretion of radioactive isoniazid in tuberculous patients. JAMA 151:1384–1388.
4. Bareggi SR, Cerutti R, Pirola R, Riva R, Cisternino M. 1987. Clinical pharmacokinetics and metabolism of pyrazinamide in healthy volunteers. Arzneimittelforschung 37:849–854.
5. Barry CE, et al. 2009. The spectrum of latent tuberculosis: rethinking the biology and intervention strategies. Nat. Rev. Microbiol. 7:845–855.
6. Canetti G, Parrot R, Porven G, Le Lirzin M. 1969. Rifomycin levels in the lung and tuberculous lesions in man. Acta Tuberc. Pneumol. Belg. 60:315–322. (In French.)
7. Carceles CM, Serrano JM, Marin P, Escudero E, Fernandez-Varon E. 2006. Pharmacokinetics of moxifloxacin in rabbits after intravenous, subcutaneous and a long-acting poloxamer 407 gel formulation administration. J. Vet. Med. A Physiol. Pathol. Clin. Med. 53:300–304.
8. Chan K, Wong CL. 1988. Pharmacokinetics of pyrazinamide in plasma and CSF of rabbits following intravenous and oral administration. Eur. J. Drug Metab. Pharmacokinet. 13:195–199.
9. Chang KC, Leung CC, Yew WW, Ho SC, Tam CM. 2004. A nested case-control study on treatment-related risk factors for early relapse of tuberculosis. Am. J. Respir. Crit. Care Med. 170:1124–1130.
10. Conte JE, Jr, Golden JA, Duncan S, McKenna E, Zurlinden E. 1999. Intrapulmonary concentrations of pyrazinamide. Antimicrob. Agents Chemother. 43:1329–1333.
11. Conte JE, Jr, et al. 2002. Effects of gender, AIDS, and acetylator status on intrapulmonary concentrations of isoniazid. Antimicrob. Agents Chemother. 46:2358–2364.
12. Dannenberg AM, Jr. 2006. Pathogenesis of human pulmonary tuberculosis. ASM Press, Washington, DC.
13. Dannenberg AM, Jr. 2006. Stages in the pathogenesis of human and rabbit tuberculosis, p 22–33. In Pathogenesis of human pulmonary tuberculosis. ASM Press, Washington, DC.
14. Ellard GA, Humphries MJ, Allen BW. 1993. Cerebrospinal fluid drug concentrations and the treatment of tuberculous meningitis. Am. Rev. Respir. Dis. 148:650–655.
15. Ellard GA, Humphries MJ, Gabriel M, Teoh R. 1987. Penetration of pyrazinamide into the cerebrospinal fluid in tuberculous meningitis. Br. Med. J. (Clin. Res. ed.) 294:284–285.
16. Eum SY, et al. 2010. Neutrophils are the predominant infected phagocytic cells in the airways of patients with active pulmonary TB. Chest 137:122–128.
17. Fernandez-Varon E, et al. 2005. Pharmacokinetic-pharmacodynamic integration of moxifloxacin in rabbits after intravenous, intramuscular and oral administration. J. Vet. Pharmacol. Ther. 28:343–348.
18. Firsov AA, et al. 2000. Comparative pharmacodynamics of moxifloxacin and levofloxacin in an in vitro dynamic model: prediction of the equivalent AUC/MIC breakpoints and equieffficient doses. J. Antimicrob. Chemother. 46:725–732.
19. Gobburu JV, et al. 2001. Pharmacokinetic-pharmacodynamic modeling of rivastigmine, a cholinesterase inhibitor, in patients with Alzheimer's disease. J. Clin. Pharmacol. 41:1082–1090.
20. Goutelle S, et al. 2009. Population modeling and Monte Carlo simulation study of the pharmacokinetics and antituberculosis pharmacodynamics of rifampin in lungs. Antimicrob. Agents Chemother. 53:2974–2981.
21. Gumbo T. 2010. New susceptibility breakpoints for first-line antituberculosis drugs based on antimicrobial pharmacokinetic/pharmacodynamic science and population pharmacokinetic variability. Antimicrob. Agents Chemother. 54:1484–1491.
22. Gumbo T, et al. 2004. Selection of a moxifloxacin dose that suppresses drug resistance in Mycobacterium tuberculosis, by use of an in vitro phar-

macodynamic infection model and mathematical modeling. J. Infect. Dis. **190**:1642–1651.

23. **Hu Y, Coates AR, Mitchison DA.** 2003. Sterilizing activities of fluoroquinolones against rifampin-tolerant populations of Mycobacterium tuberculosis. Antimicrob. Agents Chemother. **47**:653–657.

24. **Jeena PM, Bishai WR, Pasipanodya JG, Gumbo T.** 2011. In silico children and the glass mouse model: clinical trial simulations to identify and individualize optimal isoniazid doses in children with tuberculosis. Antimicrob. Agents Chemother. **55**:539–545.

25. **Jonsson EN, Karlsson MO.** 1999. Xpose—an S-PLUS based population pharmacokinetic/pharmacodynamic model building aid for NONMEM. Comput. Methods Programs Biomed. **58**:51–64.

26. **Kaplan G, et al.** 2003. Mycobacterium tuberculosis growth at the cavity surface: a microenvironment with failed immunity. Infect. Immun. **71**: 7099–7108.

27. **Kaplan G, Tsenova L.** 2011. Pulmonary tuberculosis in the rabbit, p 107–128. *In* Leong FJ, Dartois V, Dick T (ed), A color atlas of comparative pathology of pulmonary tuberculosis. CRC Press, Boca Raton, FL.

28. **Kim DH, et al.** 2008. Treatment outcomes and long-term survival in patients with extensively drug-resistant tuberculosis. Am. J. Respir. Crit. Care Med. **178**:1075–1082.

29. **Kislitsyna NA.** 1985. Comparative evaluation of rifampicin and isoniazid penetration into the pathological foci of the lungs in tuberculosis patients. Probl. Tuberk., p 55–57. (In Russian.)

30. **Kislitsyna NA, Kotova NI.** 1980. Rifampicin and isoniazid concentration in the blood and resected lungs in tuberculosis with combined use of the preparations. Probl. Tuberk., p 63–65. (In Russian.)

31. **Lee SY, Fan HW, Sutherland C, DeRyke AC, Nicolau DP.** 2007. Antibacterial effects of moxifloxacin and levofloxacin simulating epithelial lining fluid concentrations against community-acquired methicillin-resistant Staphylococcus aureus. Drugs R D **8**:69–77.

32. **Leong FJ, Eum SY, Via LE, Barry CER.** 2011. Pathology of tuberculosis in the human lung, p 53–81. *In* Dartois V, Dick T, Leong FJ (ed), A color atlas of comparative pathology of pulmonary tuberculosis. CRC Press, Boca Raton, FL.

33. **Lindbom L, Pihlgren P, Jonsson EN.** 2005. PsN-toolkit—a collection of computer intensive statistical methods for non-linear mixed effect modeling using NONMEM. Comput. Methods Programs Biomed. **79**: 241–257.

34. **Lindbom L, Ribbing J, Jonsson EN.** 2004. Perl-speaks-NONMEM (PsN)—a Perl module for NONMEM related programming. Comput. Methods Programs Biomed. **75**:85–94.

35. **Liu P, Derendorf H.** 2003. Antimicrobial tissue concentrations. Infect. Dis. Clin. North Am. **17**:599–613.

36. **Loos U, et al.** 1985. Pharmacokinetics of oral and intravenous rifampicin during chronic administration. Klin. Wochenschr. **63**:1205–1211.

37. **Mitchison DA.** 1985. The action of antituberculosis drugs in short-course chemotherapy. Tubercle **66**:219–225.

38. **Mitchison DA.** 1973. Plasma concentrations of isoniazid in the treatment of tuberculosis. *In* Davies DS, Prichard BNC (ed), Biological effects of drugs in relation to their plasma concentrations. Macmillan, New York, NY.

39. **Mitchison DA, Coates AR.** 2004. Predictive in vitro models of the sterilizing activity of anti-tuberculosis drugs. Curr. Pharm. Des. **10**:3285–3295.

40. **Mouton JW, et al.** 2008. Tissue concentrations: do we ever learn? J. Antimicrob. Chemother. **61**:235–237.

41. **Niemi M, Backman JT, Fromm MF, Neuvonen PJ, Kivisto KT.** 2003. Pharmacokinetic interactions with rifampicin: clinical relevance. Clin. Pharmacokinet. **42**:819–850.

42. **Noel AR, Bowker KE, Macgowan AP.** 2005. Pharmacodynamics of moxi-

floxacin against anaerobes studied in an in vitro pharmacokinetic model. Antimicrob. Agents Chemother. **49**:4234–4239.

43. **O'Brien JK, Doerfler ME, Harkin TJ, Rom WN.** 1998. Isoniazid levels in the bronchoalveolar lavage fluid of patients with pulmonary tuberculosis. Lung **176**:205–211.

44. **Pillai G, et al.** 2006. Population pharmacokinetics of ibandronate in Caucasian and Japanese healthy males and postmenopausal females. Int. J. Clin. Pharmacol. Ther. **44**:655–667.

45. **Piotrovskii VK.** 1987. The use of Weibull distribution to describe the in vivo absorption kinetics. J. Pharmacokinet. Biopharm. **15**:681–686.

46. **Prideaux B, et al.** 2011. High-sensitivity MALDI-MRM-MS imaging of moxifloxacin distribution in tuberculosis-infected rabbit lungs and granulomatous lesions. Anal. Chem. **83**:2112–2118.

47. **Reed MB, et al.** 2004. A glycolipid of hypervirulent tuberculosis strains that inhibits the innate immune response. Nature **431**:84–87.

48. **Sacchettini JC, Rubin EJ, Freundlich JS.** 2008. Drugs versus bugs: in pursuit of the persistent predator Mycobacterium tuberculosis. Nat. Rev. Microbiol. **6**:41–52.

49. **Sauermann R, et al.** 2005. Antibiotic abscess penetration: fosfomycin levels measured in pus and simulated concentration-time profiles. Antimicrob. Agents Chemother. **49**:4448–4454.

50. **Savic RM, Jonker DM, Kerbusch T, Karlsson MO.** 2007. Implementation of a transit compartment model for describing drug absorption in pharmacokinetic studies. J. Pharmacokinet. Pharmacodyn. **34**:711–726.

51. **Soman A, Honeybourne D, Andrews J, Jevons G, Wise R.** 1999. Concentrations of moxifloxacin in serum and pulmonary compartments following a single 400 mg oral dose in patients undergoing fibre-optic bronchoscopy. J. Antimicrob. Chemother. **44**:835–838.

52. **Stass H, Dalhoff A, Kubitza D, Schuhly U.** 1998. Pharmacokinetics, safety, and tolerability of ascending single doses of moxifloxacin, a new 8-methoxy quinolone, administered to healthy subjects. Antimicrob. Agents Chemother. **42**:2060–2065.

53. **Tunblad K, et al.** 2008. The use of clinical irrelevance criteria in covariate model building with application to dofetilide pharmacokinetic data. J. Pharmacokinet. Pharmacodyn. **35**:503–526.

54. **Via LE, et al.** 2008. Tuberculous granulomas are hypoxic in guinea pigs, rabbits, and nonhuman primates. Infect. Immun. **76**:2333–2340.

55. **Wagner C, Sauermann R, Joukhadar C.** 2006. Principles of antibiotic penetration into abscess fluid. Pharmacology **78**:1–10.

56. **Wallis RS, et al.** 1999. Drug tolerance in Mycobacterium tuberculosis. Antimicrob. Agents Chemother. **43**:2600–2606.

57. **Walubo A, Chan K, Wong CL.** 1991. The pharmacokinetics of isoniazid and hydrazine metabolite in plasma and cerebrospinal fluid of rabbits. Methods Find. Exp. Clin. Pharmacol. **13**:199–204.

58. **Walubo A, Chan K, Woo J, Chan HS, Wong CL.** 1991. The disposition of antituberculous drugs in plasma of elderly patients. II. Isoniazid, rifampicin and pyrazinamide. Methods Find. Exp. Clin. Pharmacol. **13**: 551–556.

59. **Wayne LG, Hayes LG.** 1996. An in vitro model for sequential study of shiftdown of Mycobacterium tuberculosis through two stages of nonreplicating persistence. Infect. Immun. **64**:2062–2069.

60. **Wayne LG, Sohaskey CD.** 2001. Nonreplicating persistence of Mycobacterium tuberculosis. Annu. Rev. Microbiol. **55**:139–163.

61. **WHO.** 2011. Tuberculosis MDR-TB & XDR-TB 2011 progress report. WHO, Geneva, Switzerland.

62. **Ziglam HM, Baldwin DR, Daniels I, Andrew JM, Finch RG.** 2002. Rifampicin concentrations in bronchial mucosa, epithelial lining fluid, alveolar macrophages and serum following a single 600 mg oral dose in patients undergoing fibre-optic bronchoscopy. J. Antimicrob. Chemother. **50**:1011–1015.